ANTIVIRAL DEFENSE

An isoform of Dicer protects mammalian stem cells against multiple RNA viruses

Enzo Z. Poirier[1]*, Michael D. Buck[1], Probir Chakravarty[2], Joana Carvalho[3]†, Bruno Frederico[1], Ana Cardoso[1], Lyn Healy[4], Rachel Ulferts[5], Rupert Beale[5,6], Caetano Reis e Sousa[1]*

In mammals, early resistance to viruses relies on interferons, which protect differentiated cells but not stem cells from viral replication. Many other organisms rely instead on RNA interference (RNAi) mediated by a specialized Dicer protein that cleaves viral double-stranded RNA. Whether RNAi also contributes to mammalian antiviral immunity remains controversial. We identified an isoform of Dicer, named antiviral Dicer (aviD), that protects tissue stem cells from RNA viruses—including Zika virus and severe acute respiratory syndrome coronavirus 2 (SARS-CoV-2)—by dicing viral double-stranded RNA to orchestrate antiviral RNAi. Our work sheds light on the molecular regulation of antiviral RNAi in mammalian innate immunity, in which different cell-intrinsic antiviral pathways can be tailored to the differentiation status of cells.

Type I and III innate interferons (IFNs) are rapidly induced in mammalian cells in response to virus infection. These cytokines act in an autocrine and paracrine manner to promote the transcription of multiple interferon-stimulated genes (ISGs), which encode a variety of viral restriction, cellular arrest, and cell death factors (1). The inducible protection conferred by IFN receptor signaling is much more marked in differentiated cells than in embryonic and adult stem cells, which lack expression of components of the pathways that lead to IFN induction and IFN responsiveness (2–4). This may ensure that infected stem cells are spared the cytostatic and cytotoxic effects of IFN exposure.

The IFN system is absent from invertebrates and plants, which protect themselves from viral infection by means of RNA interference (RNAi) (5). Antiviral RNAi starts with the protein Dicer, which recognizes and cleaves double-stranded RNA (dsRNA) produced during RNA virus infection to generate small interfering RNAs (siRNAs). These guide the sequence-specific degradation of viral RNAs by a slicing-active Argonaute protein such as Argonaute 2 (Ago2), present in insects and mammals. Irrespective of infection, RNAi also has a distinct role in regulating cellular gene expression through microRNAs (miRNAs) produced by Dicer cleavage of precursor miRNAs (pre-miRNAs) (5). Recent work suggests that mammals, like invertebrates and plants, can co-opt RNAi for antiviral immunity (5). Examples of mammalian antiviral RNAi in vitro and in vivo have been reported for Nodamura virus, human enterovirus 71, Zika virus, and other RNA viruses (6–14), although other studies have argued against the existence of such a response (15–18). Part of the controversy may relate to the fact that IFN inhibits mammalian dsRNA-mediated RNAi and the latter may therefore only be relevant in cells that are hyporesponsive to IFNs, such as stem cells (5, 19, 20). Notably, stem cells can resist virus infection, which has been partly attributed to IFN-independent constitutive expression of restriction factors (21). Whether stem cells additionally possess specializations that favor antiviral RNAi remains unclear.

Plants and insects that use RNAi both as a means of regulating translation of cellular mRNAs and as an antiviral mechanism encode multiple Dicers, each dedicated to one arm of the pathway. In contrast, mammals possess a single *DICER* gene with one canonical protein product, which cleaves pre-miRNA but processes dsRNA poorly (22, 23). Interestingly, a truncated form of Dicer with improved antiviral capacity can be produced from the *Dicer* gene in mice, but its expression is restricted to oocytes (24). By analogy, we hypothesized that antiviral RNAi in mammals may involve expression of an isoform of Dicer that processes dsRNA more efficiently than canonical Dicer. By performing a polymerase chain reaction (PCR) on total cDNA from mouse small intestine, we identified an alternatively spliced in-frame transcript of Dicer missing exons 7 and 8 (Fig. 1A). In silico translation of this transcript resulted in a truncated Dicer protein in which the central Hel2i domain of the N-terminal helicase segment is absent (Fig. 1A). For simplicity, hereafter we refer to canonical Dicer (which includes the sequences encoded by exons 7 and 8) as Dicer and its truncated form as antiviral Dicer (aviD). Using a reverse transcription quantitative PCR (RT-qPCR) assay that distinguishes *aviD* and *Dicer* mRNA,

both isoforms could be detected in mouse cells, including neural stem cells, embryonic stem cells (ES cells), and a 3T3 cell line, as well as in organs from pre-weaning or adult mice (fig. S1, A to D). The *AVID* and *DICER* transcripts were also found in human ES cells, human induced pluripotent stem cells (iPSCs), and some human cell lines (fig. S1, E to H). In general, transcripts encoding aviD appeared to be less abundant than transcripts encoding full-length Dicer by at least a factor of 10 (fig. S1), explaining in part why they are not easily found in public domain RNA-seq datasets. Nonetheless, they resulted in detectable protein, as immunoprecipitation using an antibody that dually recognizes Dicer and aviD demonstrated the presence of low levels of aviD protein in mouse ES cells, human iPSCs and human embryonic kidney (HEK) 293T cells (Fig. 1B) but, as expected, not in *Dicer* gene–deficient (Dicer^{−/−} aviD^{−/−}) cells used as a negative control (25, 26). aviD lacks part of the helicase domain, which negatively regulates Dicer's ability to process dsRNA (22, 23). Consistent with that notion, recombinant aviD produced about twice as much siRNA from synthetic dsRNA as did recombinant Dicer in an in vitro dicing assay (Fig. 1C). In addition, aviD was more resistant to LGP2, an ISG product that inhibits dsRNA cleavage by Dicer and is partly responsible for IFN-mediated inhibition of antiviral RNAi in differentiated mammalian cells (20) (Fig. 1D). In contrast to dsRNA cleavage, both Dicer and aviD generated equivalent amounts of *let-7a* miRNA from pre-miRNA (Fig. 1E). These results suggest that loss of the Hel2i domain does not impair the ability of aviD to process miRNA precursors but confers enhanced capacity to dice dsRNA into siRNAs, a hallmark of Dicers involved in antiviral RNAi.

To assess the ability of aviD to mediate antiviral RNAi, we complemented *Dicer* gene–deficient (Dicer^{−/−}aviD^{−/−}) HEK293T "NoDice" cells (26) by stable transfection with constructs encoding FLAG-tagged Dicer or aviD to generate sublines denoted as Dicer^{+/+}aviD^{−/−} or Dicer^{−/−}aviD^{+/+} 293T, respectively (figs. S2A and S3). By immunofluorescence, aviD and Dicer localization was predominantly cytoplasmic (fig. S3). Consistent with the in vitro pre-miRNA cleavage assays (Fig. 1E), the expression of either Dicer or aviD was sufficient to restore miRNA production to Dicer^{−/−}aviD^{−/−} "NoDice" cells (fig. S2, B and C). We then infected Dicer (Dicer^{+/+}aviD^{−/−})–expressing or aviD (Dicer^{−/−}aviD^{+/+})–expressing cells with Sindbis virus (SINV) or with Zika virus (ZIKV), two RNA viruses that are targets of antiviral RNAi in insects. We did not include Dicer^{−/−}aviD^{−/−} cells in these experiments to avoid confounding effects from loss of miRNA-regulated protein expression. Notably, cells expressing only aviD displayed lower production of SINV (Fig. 2A) and ZIKV (Fig. 2B) virus progeny than
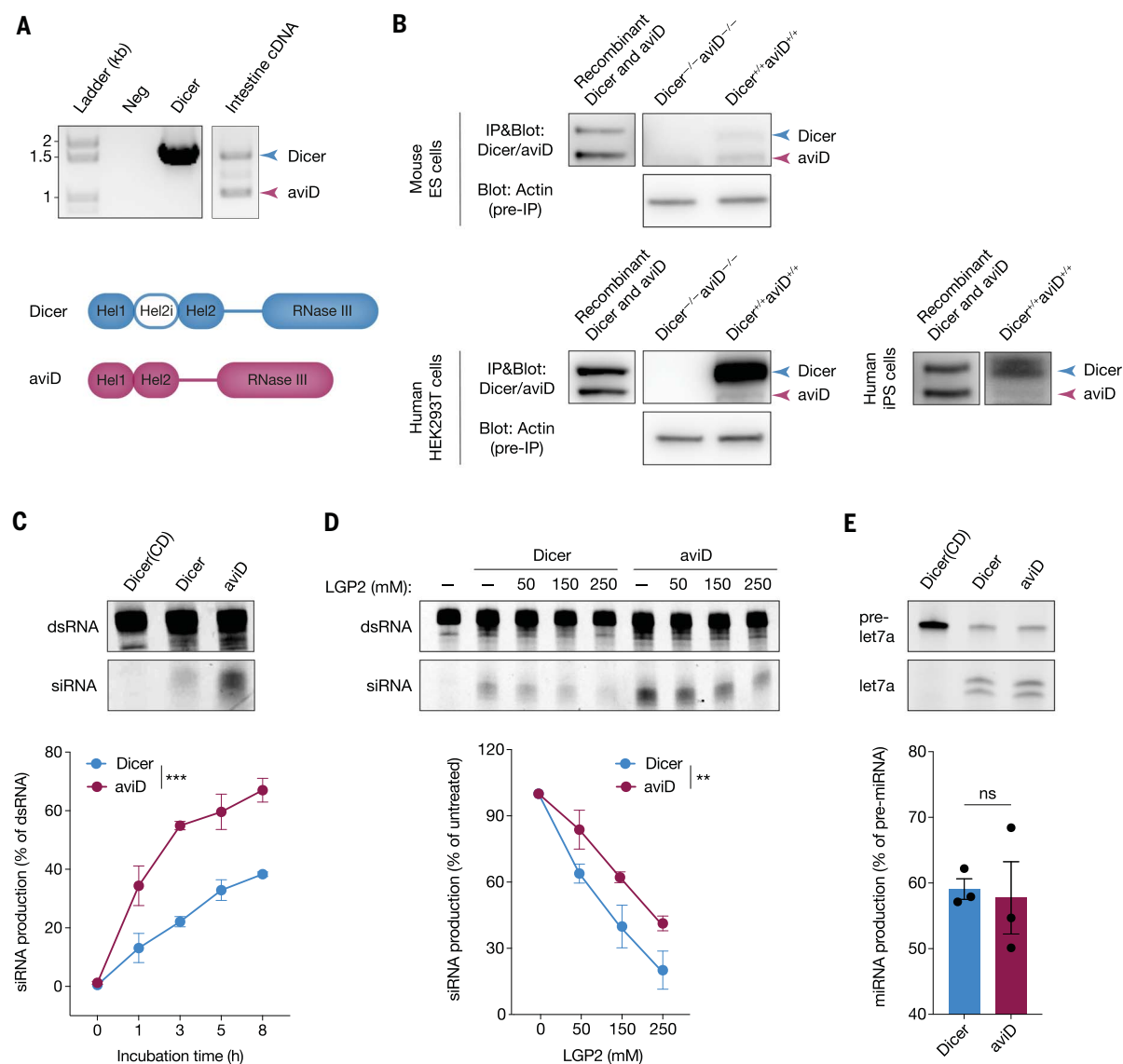
Fig. 1. aviD is an isoform of Dicer that efficiently cleaves dsRNA. (**A**) Dicer PCR amplicons using vehicle (Neg), a plasmid coding for Dicer, or mouse small intestine cDNA templates. In addition to a canonical product corresponding to full-length Dicer, an in-frame transcript missing exons 7 and 8 (nucleotides 705 to 1346 of the coding sequence) was detected. This corresponds to an isoform termed antiviral Dicer (aviD) lacking the Hel2i domain of the helicase (white). (**B**) Immunoblots from wild-type Dicer$^{+/+}$aviD$^{+/+}$ or Dicer$^{-/-}$aviD$^{-/-}$ mouse ES cells, HEK293T cells, or Dicer$^{+/+}$aviD$^{+/+}$ human iPSC lysates before (pre-IP) or after immunoprecipitation with a Dicer/aviD-specific antibody. Recombinant Flag-tagged Dicer and aviD were included as controls. (**C**) Recombinant Flag-tagged Dicer, Dicer catalytically deficient [Dicer(CD), used as a negative control], or aviD were incubated with synthetic Cy5-labeled dsRNA at 37°C for the indicated time. The reactions were resolved on a denaturing polyacrylamide gel and visualized by Cy5 in-gel fluorescence, and Dicer versus aviD cleavage was quantitated by densitometry. (**D**) Increasing concentrations of recombinant LGP2 were added to the in vitro dicing reaction as in (C) and incubated for 3 hours at 37°C. After densitometric quantitation, the siRNA amount was normalized to the amount of siRNA produced in a reaction without LGP2. (**E**) Immunopurified Flag-tagged Dicer, Dicer(CD), or aviD were incubated with *let-7a* pre-miRNA at 37°C for 20 min. The reactions were resolved on a denaturing polyacrylamide gel and visualized by Cy5 in-gel fluorescence, and Dicer versus aviD cleavage was quantitated by densitometry. Data in (C) to (E) are means ± SEM pooled from three independent experiments. **$P < 0.01$, ***$P < 0.001$ [two-way analysis of variance (ANOVA) in (C) and (D), Mann-Whitney test in (E)]; ns, not significant.

did cells that only expressed Dicer. We further tested doxycycline-inducible acute expression of the proteins in the same cells. aviD but not Dicer induction impaired SINV-GFP viral replication over time, as measured by accumulation of green fluorescent protein (GFP) (Fig. 2, C to F). This was not observed with a version of aviD that was catalytically deficient in dsRNA cleavage [aviD(CD)] (Fig. 2, C to F). These data demonstrate that aviD but not Dicer possesses antiviral function that is dependent on its catalytic domain, consistent with a role in RNAi.

Mammals encode four Ago proteins, all of which can mediate miRNA-driven gene silencing. However, only Ago2 possesses endonuclease activity to mediate target "slicing" in antiviral RNAi. Silencing Ago2 in Dicer$^{-/-}$aviD$^{+/+}$ cells (fig. S4A) rescued ZIKV particle production to levels similar to those in Dicer$^{+/+}$aviD$^{-/-}$ cells treated with control or *Ago2* siRNA (Fig. 2G). We also tested the effect of the B2 protein of Nodamura virus, a well-characterized viral suppressor of RNAi (VSR) that shields

dsRNA from Dicer cleavage (*5*, *12*). SINV-GFP and SINV expressing B2 (SINV-B2) grew to similar levels in baby hamster kidney cells (fig. S4, B and C), Dicer$^{-/-}$aviD$^{-/-}$ cells (fig. S4D), and Dicer$^{+/+}$aviD$^{-/-}$ cells (fig. S4E). In contrast, infectious virion production in Dicer$^{-/-}$aviD$^{+/+}$ cells infected with SINV-B2 was greater than in the same cells infected with SINV-GFP by as much as a factor of 100 (fig. S4F). Finally, given the current human impact of the coronavirus pandemic, we further tested the ability to resist infection by severe acute respiratory syndrome coronavirus 2 (SARS-CoV-2) in Dicer$^{+/+}$aviD$^{-/-}$ or Dicer$^{-/-}$aviD$^{+/+}$ cells that had been engineered to express the SARS-CoV-2 entry receptor ACE2 (angiotensin-converting enzyme 2) (fig. S2D). We observed a factor of 3 reduction of the number of infected Dicer$^{-/-}$aviD$^{+/+}$ cells relative to infected Dicer$^{+/+}$aviD$^{-/-}$ cells (Fig. 2H). Together, these data reveal that expression of aviD allows for an antiviral RNAi response that restricts replication of several RNA viruses. In contrast, replication of two DNA viruses, vaccinia virus and herpes simplex virus 1, was similar in Dicer$^{+/+}$aviD$^{-/-}$ and Dicer$^{-/-}$aviD$^{+/+}$ cells (fig. S4, G and H).

We examined the expression of aviD in mice. aviD transcripts could be detected by fluorescence in situ hybridization (fig. S5A) in the crypts of mouse small intestine, where they colocalized with Lgr5, a marker of intestinal stem cells, but were not found in differentiated cells along the villi (Fig. 3A). By PrimeFlow cytometry, validated using complemented Dicer$^{-/-}$aviD$^{-/-}$ HEK293T cells (fig. S5B), *aviD* mRNA was found to be predominantly expressed in a fraction of Lgr5$^+$ stem cells in the intestine, as well as in Lgr5$^+$ hair follicle stem cells of the skin and in Sox2$^+$ neural stem cells of the hippocampus (Fig. 3B). Consistent with the latter, *aviD* expression by RT-qPCR was found in cultured neural stem cells but, unlike *Dicer* mRNA, was lost when the cells were made to differentiate into astrocytes (fig. S5C). These data suggest that aviD is expressed preferentially by stem cells rather than differentiated cells within adult mouse tissues.

To assess the role of aviD in stem cells, we took advantage of an in vitro model of organ generation using ES cells. We complemented mouse Dicer$^{-/-}$aviD$^{-/-}$ ES cells (*25*) with either Dicer or aviD (fig. S6A). The interferon unresponsiveness of ES cells relies in part on their production of miR-673, which inhibits MAVS (mitochondrial antiviral signaling protein) to block coupling of RNA virus detection to IFN gene transcription (*2*). As a consequence, ES Dicer$^{-/-}$aviD$^{-/-}$ cells lacking miRNAs produce type I interferons and transcribe ISGs in response to viral stimulation, unlike their wild-type counterparts (*2*). We confirmed that introduction of either Dicer or aviD into Dicer$^{-/-}$aviD$^{-/-}$ ES cells restored miRNA production, including that of miR-673, and inhibited the induction
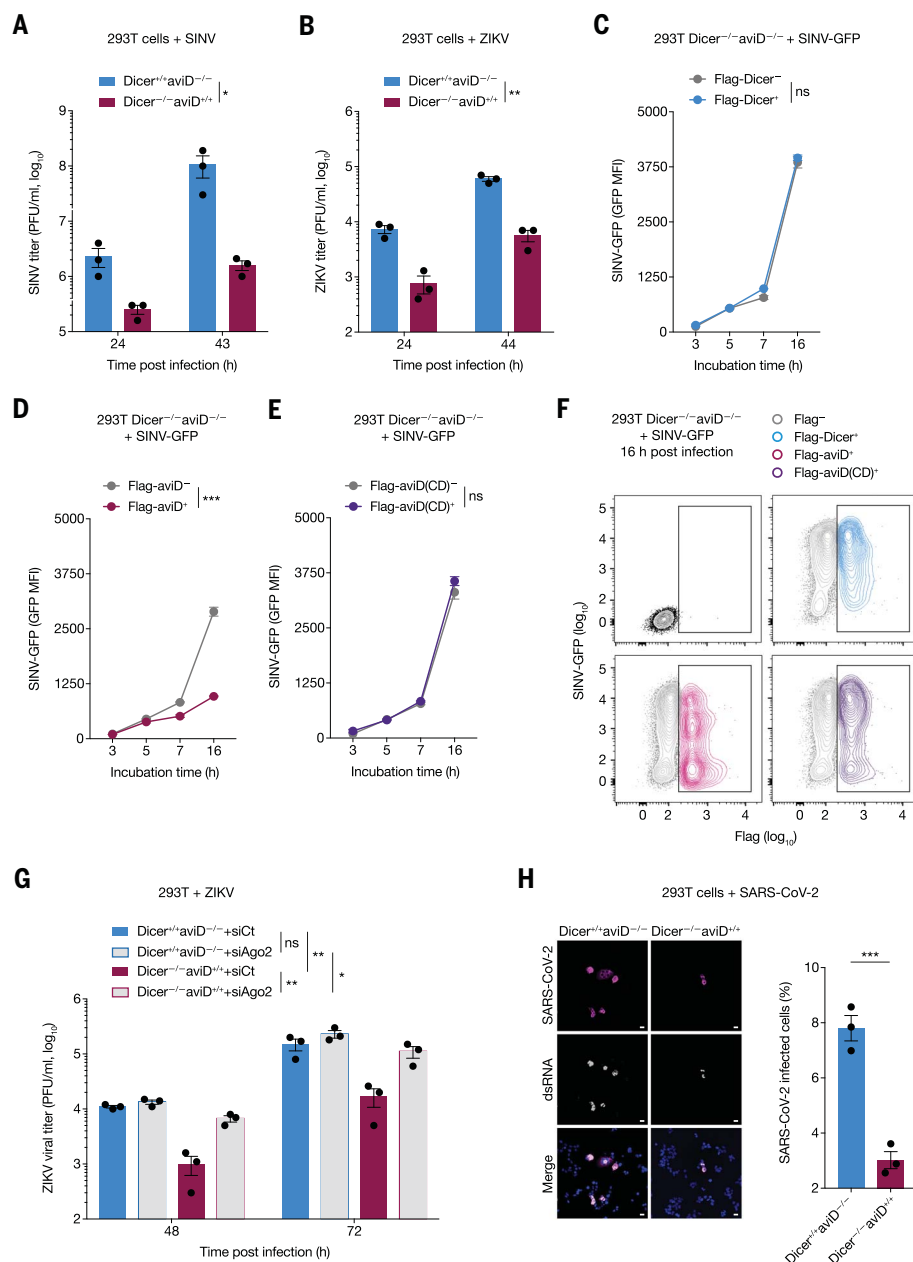

Fig. 2. aviD can mediate antiviral RNAi. (A and **B)** HEK293T Dicer$^{-/-}$aviD$^{-/-}$ cells complemented with Dicer (Dicer$^{+/+}$aviD$^{-/-}$) or aviD (Dicer$^{-/-}$aviD$^{+/+}$) were infected with SINV (A) or ZIKV (B) at MOI (multiplicity of infection) of 0.1. Supernatant was collected at the indicated time points and viral content determined by plaque assay. **(C** to **E)** HEK293T Dicer$^{-/-}$aviD$^{-/-}$ cells induced by doxycycline to express Flag-Dicer (C), aviD (D), or aviD(CD) (E) were infected with SINV-GFP. Flow cytometry was used to monitor the expression of Dicer/aviD (via anti-Flag staining) and SINV replication (via GFP fluorescence). **(F)** Representative contour plots from 16 hours after infection. Boxes represent Flag-positive cells defined on the basis of the uninduced controls (top left plot). **(G)** Dicer$^{+/+}$aviD$^{-/-}$or Dicer$^{-/-}$aviD$^{+/+}$ HEK293T cells were transfected with siRNA targeting Ago2 (siAgo2) or with control siRNA (siCt) and infected with ZIKV at MOI of 0.1. Supernatant was collected at the indicated time points and viral content was determined by plaque assay. **(H)** Immunofluorescence of Dicer$^{-/-}$aviD$^{+/+}$ Dicer$^{+/+}$aviD$^{-/-}$ HEK293T cells expressing ACE2 infected with SARS-CoV-2 and stained for SARS-CoV-2 N protein (magenta) and dsRNA (white). Scale bar, 20 μm. Graph shows percentage of infected cells. Data in all panels are from one of three independent experiments. Data are means ± SEM; *n* = 3 biological replicates. *$P < 0.05$, **$P < 0.01$, ***$P < 0.001$ [unpaired *t* test (H), two-way ANOVA (other panels)].

Fig. 3. *aviD* mRNA is enriched in tissue stem cells. (**A**) Small intestine from an Lgr5-GFP reporter mouse was fixed, sectioned, and probed for *aviD* mRNA (magenta) by fluorescence in situ hybridization. The *aviD* probe was designed to detect the exon-exon junction specific to *aviD* and cannot detect *Dicer* mRNA (fig. S5A). Lgr5$^+$ stem cells were identified with anti-GFP (white) and nuclei were visualized by DNA staining (Hoechst, blue). Scale bar, 30 μm. Percentages of stem (Lgr5$^+$) or differentiated (Lgr5$^-$) cells expressing aviD mRNA were determined on 17 images with at least three villi each. Data are means ± SEM. ***$P < 0.001$ (Mann-Whitney test). (**B**) *aviD* or *Dicer* mRNA was measured by PrimeFlow cytometry in stem (Lgr5$^+$) or differentiated (Lgr5$^-$) cells from small intestine or skin isolated from Lgr5-GFP reporter mice or in stem or differentiated cells from hippocampus distinguished by the presence or absence of *Sox2* mRNA, respectively.
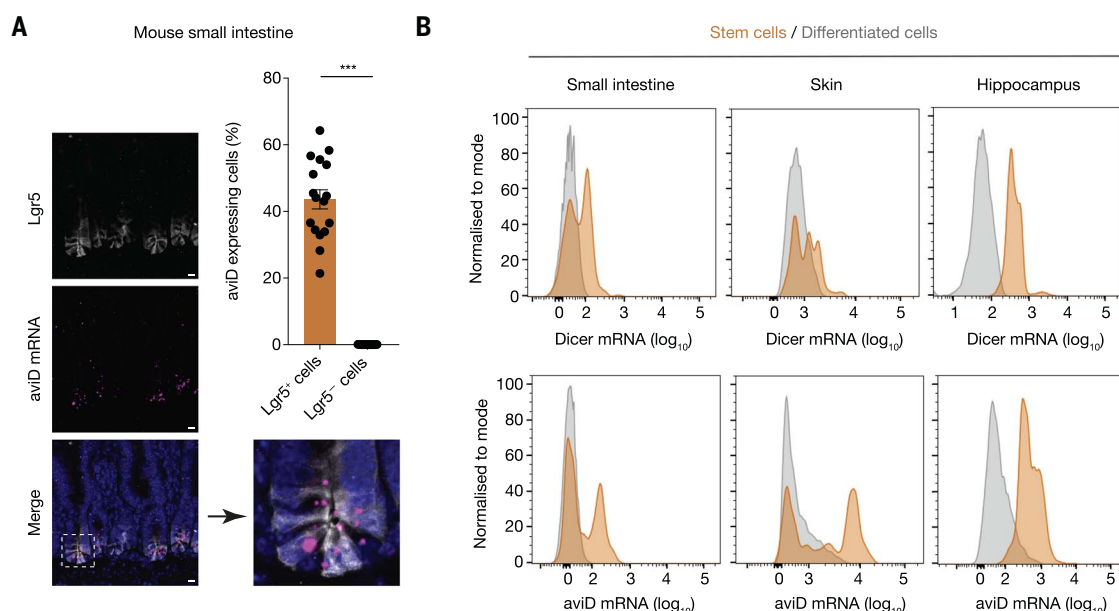
of ISGs in response to cell stimulation with a viral RNA mimic (fig. S6, B to E). Complementation with Dicer or aviD additionally suppressed the constitutive activation of protein kinase R (PKR) that has been reported to result from *Dicer* loss (27) and inhibits growth (fig. S7A). Finally, we found that aviD could also mediate dsRNA-induced gene silencing in ES cells (fig. S7B) (19).

Brain organoids derived from ES cells recapitulate the overall organization of the adult brain (28), and Sox2$^+$ neural stem cells present in organoids derived from wild-type (Dicer$^{+/+}$aviD$^{+/+}$) ES cells expressed more aviD and Dicer transcripts than differentiated cells in the same tissue (fig. S8A). Both Dicer$^{-/-}$aviD$^{+/+}$ and Dicer$^{+/+}$aviD$^{-/-}$ ES cells generated organoids similar to those made by wild-type Dicer$^{+/+}$aviD$^{+/+}$ ES cells, including differentiated neuronal layers and astrocytes (fig. S8B). ZIKV infection of brain organoids preferentially targets Sox2$^+$ stem cells, resulting in slower organoid growth and increased stem cell demise by apoptosis, which recapitulates the microcephaly phenotype observed in humans (29). Uninfected organoids grew similarly irrespective of genotype (fig. S8C). In contrast, upon infection with ZIKV, Dicer$^{+/+}$aviD$^{-/-}$ organoids grew more slowly than Dicer$^{+/+}$aviD$^{+/+}$ and Dicer$^{-/-}$aviD$^{+/+}$ organoids (Fig. 4A) and produced more infectious viral particles (Fig. 4B). Thus, despite being expressed at low levels (Fig.1B), endogenous aviD in Dicer$^{+/+}$aviD$^{+/+}$ organoids can display antiviral activity equivalent to that of ectopically expressed aviD in Dicer$^{-/-}$aviD$^{+/+}$ organoids. Consistent with the notion that absence of aviD compromises stem cell resistance to viral

infection, Sox2$^+$ stem cells in Dicer$^{+/+}$aviD$^{-/-}$ organoids displayed increased infection with ZIKV (Fig. 4C); accumulated more viral dsRNA, the substrate for aviD (Fig. 4D); and displayed decreased 5-ethynyl-2′-deoxyuridine (EdU) incorporation indicative of lower proliferation (Fig. 4E). ZIKV-derived small RNAs from infected organoids displayed canonical features of viral siRNAs, such as a predominant length of 22 nucleotides (nt) and a read-phasing consistent with the presence of 2-nt 3′ overhangs (fig. S9, A to D). Dicer$^{+/+}$aviD$^{-/-}$ organoids showed decreased accumulation of these viral siRNAs (fig. S9B), consistent with impaired ability to restrict ZIKV infection. SARS-CoV-2 can also display brain tropism and infect brain organoids (30). We engineered ES cells to express ACE2 (fig. S8D) and infected organoids with SARS-CoV-2. As for ZIKV infection, the absence of aviD in Dicer$^{+/+}$aviD$^{-/-}$ organoids correlated with an increase in the percentage of virally infected stem cells (Fig. 4F) as well as loss of viral siRNA production (fig. S9E). Taken together, these data indicate that aviD can protect adult stem cells from ZIKV and SARS-CoV-2 virus infection by orchestrating an antiviral RNAi response.

Our results show that the *DICER* gene can generate an alternative transcript that encodes aviD, a truncated Dicer that helps protect mouse and human stem cells against RNA virus infection and compensates in part for stem cell hyporesponsiveness to innate IFNs. Our data reveal that mammals, like plants or insects, can produce at least two Dicer proteins, one of which is superior at initiating antiviral RNAi. Interestingly, aviD can also

process pre-miRNAs and compensates for Dicer loss in miRNA generation when it is the only isoform expressed in the cell; this would imply that aviD is not fully specialized for antiviral RNAi. Antiviral RNAi has been noted in some studies with differentiated cells, especially when using viruses deficient in VSRs (8–10, 12–14). Whether such observations were due to aviD activity is unknown, as our data suggest that aviD is expressed only at low levels in differentiated cells. Why this should be the case is unclear. However, one element to consider is the interplay between antiviral RNAi and the IFN response (5, 19, 20). The action of aviD could deplete infected cells of viral dsRNA, thereby eliminating a key trigger of dsRNA-activated proteins of the IFN response pathway such as RIG-I, MDA5, PKR, or ribonuclease (RNase) L. This is less important for stem cells that are not reliant on the IFN pathway for antiviral resistance. Notably, aviD-mediated antiviral RNAi is not the only defense mechanism in stem cells and likely acts in concert with others conferred by IFN-independent expression of restriction factors encoded by ISGs (21). An aviD-specific knockout mouse will help to delineate the nonredundant contributions of these distinct strategies. Antiviral innate immunity in mammals is therefore a composite of pathways that are tailored to the differentiation status of the cell and that display complementarity as well as redundancy.

REFERENCES AND NOTES

1. D. Goubau, S. Deddouche, C. Reis e Sousa, *Immunity* **38**, 855–869 (2013).

Fig. 4. aviD thwarts viral infection in stem cells.
(**A**) Individual Dicer$^{+/+}$aviD$^{+/+}$, Dicer$^{+/+}$aviD$^{-/-}$, or Dicer$^{-/-}$ aviD$^{+/+}$ brain organoids were infected with ZIKV, and organoid area was monitored for 4 days. Immunofluorescent staining and confocal microscopy on organoid sections were carried out to identify stem cells by Sox2 expression (green) and infected cells by ZIKV glycoprotein expression (magenta). Scale bar, 100 μm. (**B**) Production of viral particles from ZIKV-infected organoids was determined by transferring individual organoids into fresh medium at day 3 after infection and collecting the supernatant 24 hours thereafter to determine viral content by plaque assay. In (A) and (B), $n = 16$ organoids per condition. (**C**) Percentage of ZIKV-infected stem cells was measured 4 days after infection by immunofluorescence on organoid sections. (**D**) dsRNA in infected stem cells was visualized by immunofluorescence on organoid sections after 4 days of infection. Images show dsRNA (gray) in ZIKV-infected (magenta) stem cells (green). Scale bar, 20 μm. (**E**) Stem cell division rate was measured by pulsing organoids with EdU at day 3 for 1 hour and chasing for 24 hours. Organoid sections were analyzed by immunofluorescence, with Sox2 staining to identify stem cells and EdU staining to mark cells in S phase at time of pulsing. In (C) to (E), $n = 8$ organoids per condition, 8 with highest fold change in area at day 4 for Dicer$^{+/+}$aviD$^{+/+}$ and Dicer$^{-/-}$aviD$^{+/+}$, 8 with lowest fold change in area for Dicer$^{+/+}$aviD$^{-/-}$. (**F**) Dicer$^{+/+}$aviD$^{+/+}$, Dicer$^{+/+}$aviD$^{-/-}$, or Dicer$^{-/-}$aviD$^{+/+}$ brain organoids expressing ACE2 were infected with SARS-CoV-2 for 48 hours. Percentage of infected stem cells ($n = 11$ organoids per condition) was determined by immunofluorescence on sections stained for the stem cell marker Sox2 (green) and for the SARS-CoV-2 N protein (magenta). Scale bar, 100 μm. Data are means ± SEM. *$P < 0.05$, ***$P < 0.001$ [two-way ANOVA in (A), Mann-Whitney test in (B) to (F)].
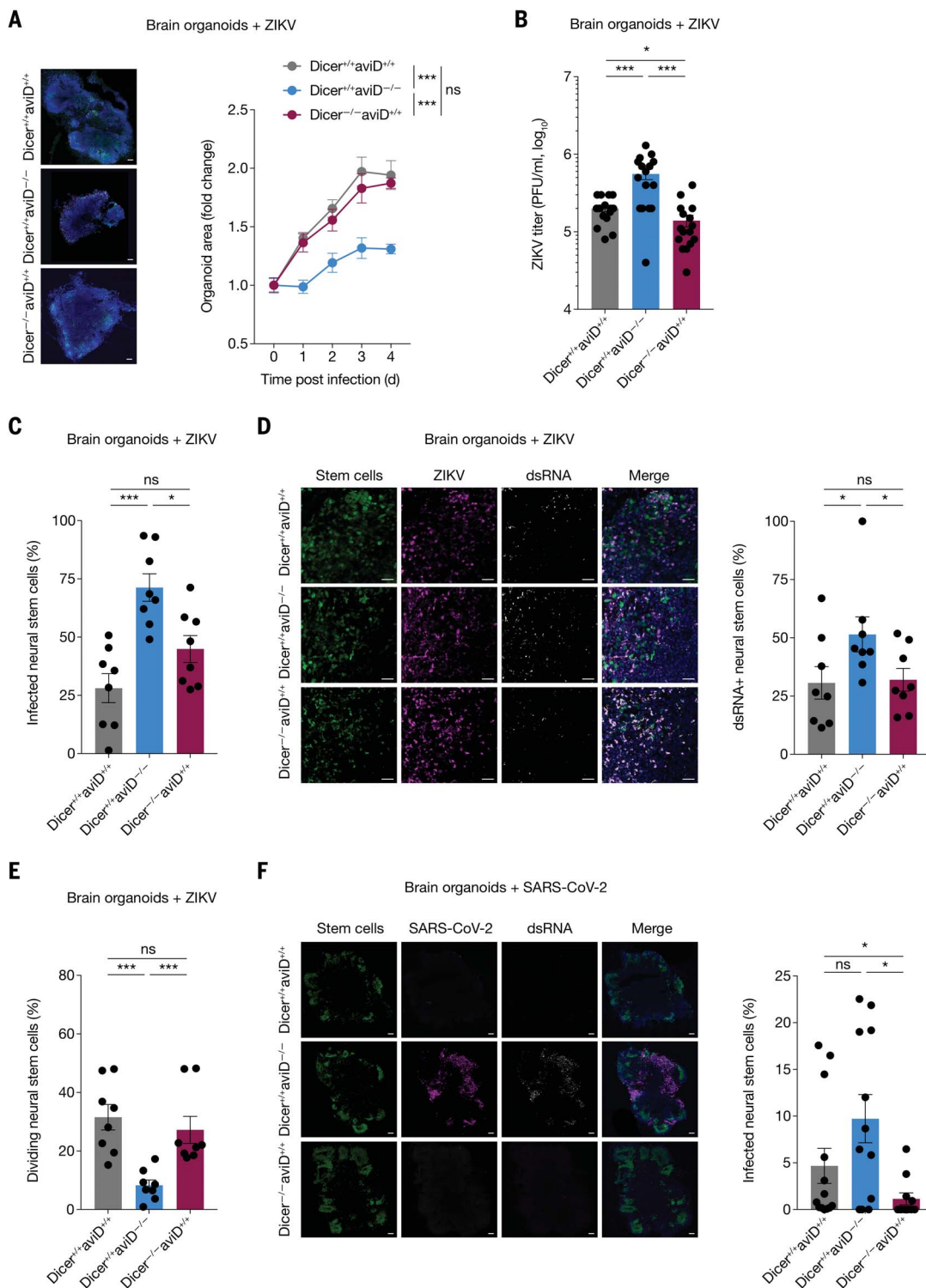
2. J. Witteveldt, L. I. Knol, S. Macias, *eLife* **8**, e44171 (2019).
3. W. D'Angelo *et al.*, *J. Immunol.* **198**, 2147–2155 (2017).
4. X.-X. Hong, G. G. Carmichael, *J. Biol. Chem.* **288**, 16196–16205 (2013).
5. P. V. Maillard, A. G. van der Veen, E. Z. Poirier, C. Reis e Sousa, *EMBO J.* **38**, e100941 (2019).
6. P. V. Maillard *et al.*, *Science* **342**, 235–238 (2013).
7. Y. Li, J. Lu, Y. Han, X. Fan, S.-W. Ding, *Science* **342**, 231–234 (2013).
8. Y. Li *et al.*, *Nat. Microbiol.* **2**, 16250 (2016).
9. Y. Qiu *et al.*, *Immunity* **46**, 992–1004.e5 (2017).
10. Q. Qian *et al.*, *J. Virol.* **94**, e01233-19 (2019).
11. Y.-P. Xu *et al.*, *Cell Res.* **29**, 265–273 (2019).
12. Q. Han *et al.*, *mBio* **11**, e03278-19 (2020).
13. Y. Zhang *et al.*, *Emerg. Microbes Infect.* **9**, 1580–1589 (2020).
14. Y. Qiu *et al.*, *Sci. Adv.* **6**, eaax7989 (2020).
15. B. R. Cullen, S. Cherry, B. R. tenOever, *Cell Host Microbe* **14**, 374–378 (2013).

16. S. Schuster, L. E. Tholen, G. J. Overheul, F. J. M. van Kuppeveld, R. P. van Rij, *MSphere* **2**, e00333-17 (2017).
17. K. Tsai, D. G. Courtney, E. M. Kennedy, B. R. Cullen, *RNA* **24**, 1172–1182 (2018).
18. S. Schuster, G. J. Overheul, L. Bauer, F. J. M. van Kuppeveld, R. P. van Rij, *Sci. Rep.* **9**, 13752 (2019).
19. P. V. Maillard *et al.*, *EMBO J.* **35**, 2505–2518 (2016).
20. A. G. van der Veen *et al.*, *EMBO J.* **37**, 97479 (2018).
21. X. Wu *et al.*, *Cell* **172**, 423–438.e25 (2017).
22. E. Ma, I. J. MacRae, J. F. Kirsch, J. A. Doudna, *J. Mol. Biol.* **380**, 237–243 (2008).
23. E. M. Kennedy *et al.*, *Proc. Natl. Acad. Sci. U.S.A.* **112**, E6945–E6954 (2015).
24. M. Flemr *et al.*, *Cell* **155**, 807–816 (2013).
25. J. E. Babiarz, J. G. Ruby, Y. Wang, D. P. Bartel, R. Blelloch, *Genes Dev.* **22**, 2773–2785 (2008).
26. H. P. Bogerd, A. W. Whisnant, E. M. Kennedy, O. Flores, B. R. Cullen, *RNA* **20**, 923–937 (2014).
27. C. Gurung *et al.*, *J. Biol. Chem.* **296**, 100264 (2021).
28. M. A. Lancaster *et al.*, *Nature* **501**, 373–379 (2013).
29. P. P. Garcez *et al.*, *Science* **352**, 816–818 (2016).
30. C. Iadecola, J. Anrather, H. Kamel, *Cell* **183**, 16–27.e1 (2020).